IFPRI Report- ARR-46-10
Simplified industrial formulations.
Design challenges

Jan Vermant and Lucio Isa,
Department of Materials, ETH Zurich

May 21, 2024

1 Goals

Overall the work in our IFPRI project has focused on how, moving away from model systems containing spherical colloids with near hard interactions, we can widen the range of rheological responses by changing the properties of the building blocks of the suspensions, so that even in simple formulations a wide range of behaviors can be "built in", i.e. obtaining formulation guidelines to do "more with less" or simplifying formulations from within. At the same time we use novel experimental methods. We also developed a constitutive model for simplified industrial suspensions, based on insights from the advanced rheological methods (stress de-convolution) and using models taking into account plastic flow behaviour using an Eyring like approach and a viscoelastic upper convected Maxwell model.

For the second IFPRI period we now focus on :

1. Particle roughness has been identified to generate surprising effects in colloidal gels and could both be tool to engineer materials from within for rheology or gravitational stability. The effect of roughness will now be explored more systematically. For gravitational stability, we will also study combined effects of roughness and shape.
2. A full study of the structural evolution of systems in (1) will be investigated by 4D confocal rheology, with an emphasis on understanding the yielding transition.
3. To understand the role of non-central forces we would intensify the measurements of local scale mechanics using AFM (to characterize static friction) and then go to the micro mechanics of model aggregates (using optical tweezers).
4. we propose to also study these systems in 2D as this also has application to engineer strong interfaces or understand what happens in protein solutions, as a model

system for lock and key interactions. The 2D nature of these systems makes them also a stepping stone for doing the micromechanics not immediately on the 3D systems.

5. we propose to continue the investigation of simplified industrial dispersion by industrial partners especially in light of systems with roughness and shape variations (e.g. a Paracetamol dispersion)

2 Imparting toughness in colloidal gels

2.1 Non-Central Interactions Induced by a Patchy Grafting Layer,

In this work[1], we first checked how universal the effect of non central forces on imparting thoughness is, and synthesized patchy particles, which arguably have somewhat ill-defined patches, both in size of the patches and number of patchy regions, that nevertheless form 3D colloidal gels that show interesting properties. This section first details the synthesis and characterization of the particles, before investigating viscoelastic properties of these particles in a gelled state. The patchy particle gel is then compared to the rheological properties of previously reported smooth and rough particle gels of comparable size and volume fractions [1].

Particles with a patchy distribution of octadecyl on a silica are synthesized by first forming particles using the Stöber process (see figure 1a.) and then slowly adding triethyl(octadecyl)silane (TMOS, see figure 1b.) to the particle suspension. The siloxane groups of the TMOS can hydrolyze in the presence of water, forming silanol groups that can react with the hydroxyl surface groups on the surface of the silica particle (see figure 1c.). This reaction is ubiquidous in literature [2–4], Badley et al. report that this grafting approach forms a stable suspension in benzene, which would indicate a homogeneous layer that allows steric hindrance [5]. However, the same authors also report that for a higher concentration of TMOS, no stable suspension can be formed, which could be attributed to a patchy distribution. They also state that reasons for this could be the attachment of the octadecyl chain to the silica particle through hydrophobic forces, oligomerization or micelle formation (see figure 1c. ii.) [5]. Another mechanism could be due to the byproduct of the condensation reaction (H_2O) as the octadecyl tail of the TMOS is hydrophobic, this might hinder further TMOS to connect to an existing patch. The silanol groups cannot only condensate to the particle, but also to other TMOS molecules, which might be the reason that molecules that already formed a chain can graft to the particle's surface in a patch. The size, distribution and amount of patches does not seem very well controllable in this synthesis method, but the inhomogeneity of the distribution is given throughout the sample (see figure 1c. iii.). Apart from coating silica particles, this approach has also been used for coating glass surfaces or silicon surfaces with TMOS, this was shown to yield superhydrophobic surfaces [6].

[1] This work builds further on the work of graduate student Florence Müller, who will defend her thesis on May 30th, 2024

For macroscopic effects, a patchy coating might be sufficient, especially for superhydrophobic applications, a patchy distribution might even enhance super-hydrophobicity as the patch induced a nano-roughness that can cause a Cassie-Baxter state for the droplet [7].

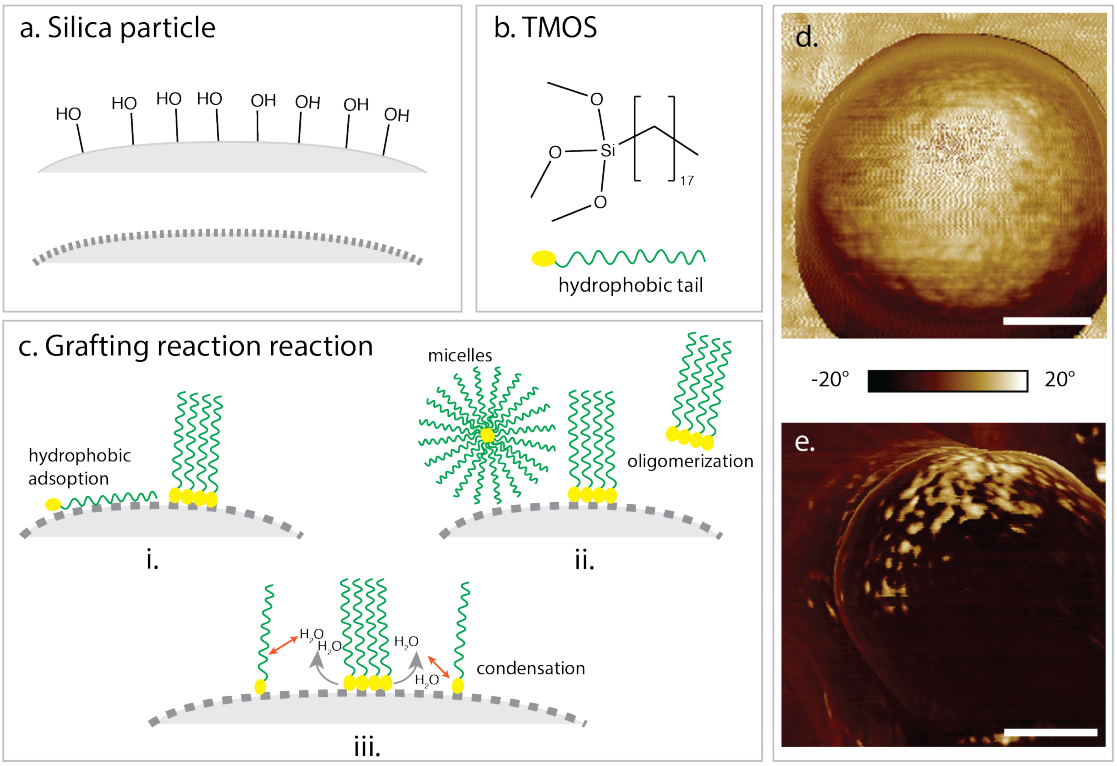

Figure 1: **Synthesis and characterization of SiO_2-octadecyl patchy particles.** a. Silica particle synthesized with the Stöber process showing hydroxyl surface groups, b. Amphiphilic triethyl(octadecyl)silane (TMOS) grafting agent, c. Condensation reaction of TMOS to the surface of the particle in a patchy surface coverage due to the hydrophopic tail, d. AFM phase imaging for the homogeneously grafted silica particles using click chemistry [1], e. AFM phase imaging for the patchy grafted particles where the bright spots indicate the TMOS and the darker spots indicate the harder silica. The scale bars correspond to 100 nm.

Depending on the nature of the patch, different characterization methods can be used to asses the distribution of the patches. For patches of heights larger than 10 nm, methods such as SEM and TEM can be used [8], but an oligomer patch would not be detectable optically. One way to render a patch visible is to adsorb smaller particles to either the patch or the bare surface, depending on the specific chemistry [9]. Conventional atomic force microscopy (AFM), similarly to electron microscopy would not necessarily detect a height difference of the order of a few nanometers, but as the mechanical properties of the particle and the patch are different, AFM phase imaging can be used to detect the

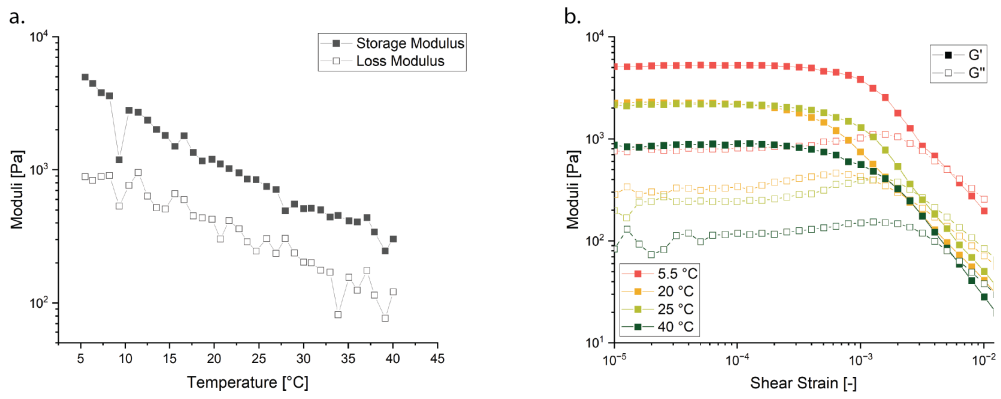

Figure 2: **Temperature dependent properties of the patchy particle suspension.** a. Temperature sweep showing a reduction in modulus but not a fluidification upon heating of the sample, b. Strain amplitude sweep at 5.5 °C, 20 °C, 25 °C and 40 °C all indicating a distinct linear viscoelastic region, showing a developed network throughout the whole temperature range.

phase shift in the needle oscillations [10]. Figure 1d. and e. show such images, where the colors indicate the phase shift, generally, negative shifts indicate a harder surface and positive shifts indicate a soft surface. Figure 1d. represents phase imaging of a homogeneously coated silica particle using the click-like chemistry reported in previous work [1], where a positive phase shift which is homogeneous throughout the whole surface shows a uniform coating. Figure 1e. shows the patchy particle, where there are a few bright patches representing a softer surface than the rest of the particle. The phase shift on these surfaces can also be quantified, in which the homogeneously coated particle has a phase shift of 12.75 $\pm$ 2.2 throughout the image, while the silica portion of the particle has a phase shift of -12.05 $\pm$ 2.93 and the octadecyl patch has a phase shift of 9.16 $\pm$ 3.1.

Figure 2 shows that the gel made out of patchy octadecyl coated particles in tetradecane is not thermoreversible. The temperature sweep (see figure 2a.), while showing a decrease in modulus, does not show a fluidification upon heating like the thermoreversible gels coated through the click-like [1]. In fact, figure 2b. even shows that for elevated temperatures, the samples have a distinct linear viscoelastic region, which proves the presence of a microstructural network. These experiments are and indication, that adjacent particles will most probably touch through two octadecyl patches. The van der Waals (vdW) interactions between two bare silica patches will not be high enough to induce a self sustaining network. The aggregation mechanism of the particles described in literature [11], show that there is interdigitation of tetradecane and the octadecyl brush as the octadecyl solidifies, increasing the vdW forces. Therefore, a bare silica patch and an octadecyl patch will have less vdW interactions as well as less of an influence on the networks elasticity. An indication that the contact might be between two octadecyl

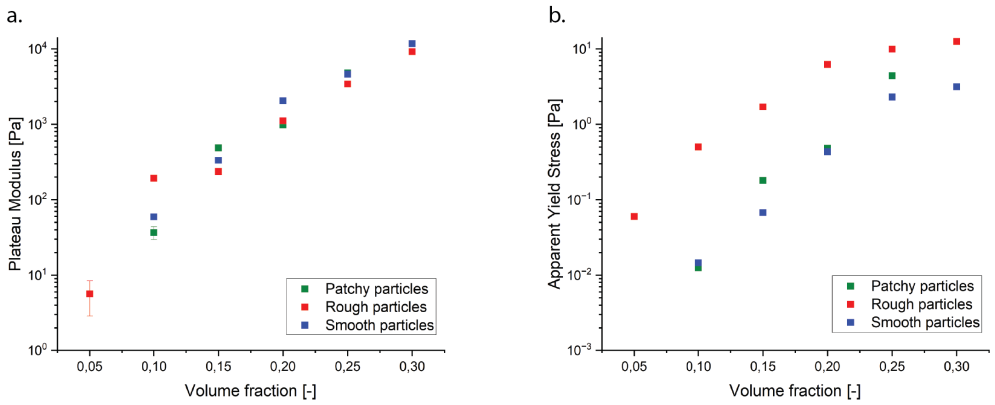

Figure 3: **Overview over the oscillatory characterization at 5.5°C, compared to the rough and smooth particle gels from chapter ??.** a. Elastic plateau modulus for the smooth, rough and patchy particles for different volume fractions, b. Apparent yield stress for the smooth, rough and patchy particles for different volume fractions.

patches is that the gels modulus decreases but the network remains. This means that the vdW interactions decrease but do not fade due to a lack of steric hindrance, which can only occur when the grafted layer is homogeneous. This question will however need to be further investigated, for instance with a more thorough colloidal probe AFM or optical tweezer study.

We can now compare the rheological behavior of the patchy particles with the smooth and rough system reported previously. All three types of particles have a hydrodynamic radius of 300 nm, which makes them comparable. Previous work (see Simplified Industrial Formulations of Colloidal Dispersions, IFPRI FRR-46-11, 2023) stated that the elastic plateau modulus of rough and smooth particles is comparable, because the microstructure in the linear viscoelastic region is the same (due to a similar kinetic pathway of aggregation) and the vdW interactions are equivalent, as they are both coated with octadecyl [1]. Figure 3a. shows that the elastic plateau modulus for the patchy particles is very similar to the rough and smooth particles, which is a further indication that the patches that interact between particles are most likely octadecyl-octadecyl. Comparing the apparent yield stress from the oscillatory measurements of the smooth, rough and patchy particles, figure 3b. shows that the patchy particles have a behavior that is in between the smooth and rough particle gels. This is an indication that the patchy particles must have some kind of non-central frictional force due to the patches. Of course, the force will be smaller than a physical mechanical roughness that leads to interlocking, but the fact that the apparent yield stress is increased from the smooth particles, while keeping the plateau modulus equal is an indication that the microstructure remains more open upon shearing.

This is also shown in the creep experiments, where the low stress response is similar to the

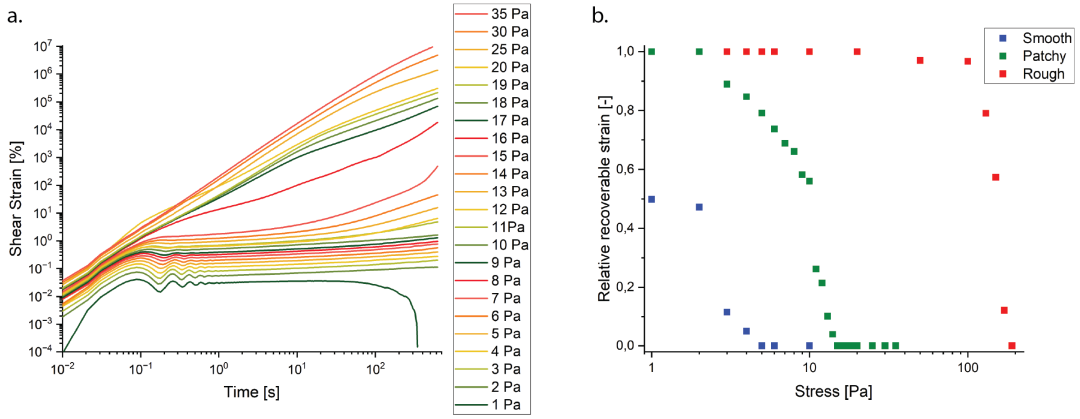

Figure 4: **Creep and recovery experiments for the patchy particles at ϕ=0.25 and 5.5 °C.** a. Creep experiment of the patchy particles, where the sample shows a rough-like behavior for low stresses and a smooth-like behavior for high stresses, b. Elastic recovery after the creep stresses for the smooth, rough and patchy particles.

one of the rough particle gel, shown by the increasing slope until 15 Pa. The difference to the rough particle creep measurements is that there is no dramatic fluidification, which would be such an abrupt decrease. This is because there is no interlocking and when the critical stress is exceeded, the particles can densify, for stresses above 16 Pa. For these stresses the curve has a characteristic shape for the smooth creep curve, where the slope decreases with time, similar to smooth particle gel in previous work. This shows that the patchy particles have an intermediate behavior between smooth and rough particle gels. This is also shown clearly in the relative stress recovery plot in figure 4b., where the recovery after creep is shown for smooth, rough and patchy particle gels of $\phi = 0.25$ at 5.5°C. The recoverable strain is an indication of elasticity of the structure, and for patchy particles it is in between the smooth and rough gels, because the more non-central forces can be applied, the more elastic the structure is, which is clearly shown in 4b.. The ability for a network to accommodate for a deformation and recover elastically, is likely to be due to homogeneity in the network structure. The fact that patchy particles with non-central forces can take up more of an elastic deformation, shows the importance inducing a homogeneous stress distribution in the gel network. We hypothesize that this is due to the fact that the frictional contact points, distruibute the load better.

Finally, the thixotropic recovery of the patchy particle gel has been investigated in oscillatory mode. Here, the structure was sheared at 100 % strain and then left to recover in the linear viscoelastic region, similar to the experiments presented in previous work [1], figure **??**a. and f. for the smooth and rough particle gel, respectively. Figure 5a. shows that the structure reforms quickly after the shear forces subside and that the signal is steady, but the microstructure does not further evolve which is shown by a constant storage modulus. Figure 5b. compares the recovery curve for patchy particles to the ones for smooth and rough particles by looking at the time evolution. It is apparent,

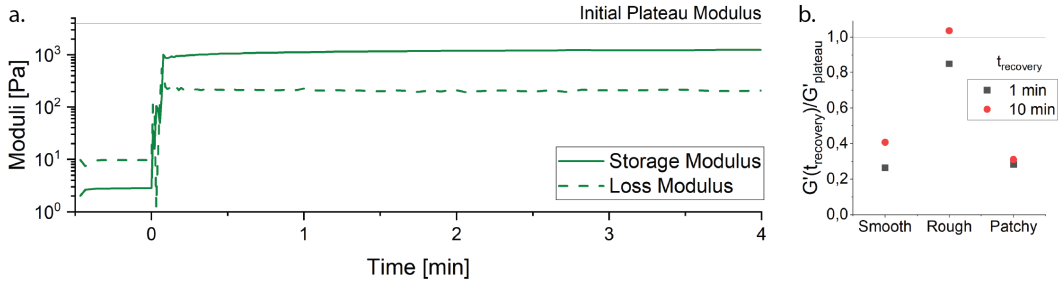

Figure 5: **Oscillatory recovery experiments.** a. Recovery after 30 s of shearing at 100 % strain and subsequent recovery in the linear viscoelastic region where the horizontal line indicates the initial plateau modulus, b. Relative modulus normalized by the respective initial plateau modulus after 1 min and 10 min of recovery for the smooth, rough and patchy particles.

that the smooth and rough particle gel both have a temporal evolution after shearing, because the relative plateau modulus is increasing after fluidification of the structure, which is less developed in the patchy particle gel. While the final recovery of the patchy particles is less than for the smooth particle gel, it is however comparable, showing that there must be some shear densification that leads to thixotropy.

While being somewhat ill-controlled, the patchy particle synthesis is very straight forward and allows for a high yield. This enables the use of these particles in bulk systems such as colloidal gels, where several milliliters of gel can easily be produced with one batch. Despite the lack of control over the number, shape and distribution of the patches, the rheological properties are very interesting and seem to fit very well with colloidal gel data of smooth and rough particles of comparable size. The plateau modulus of the patchy particles is similar to the smooth and rough particles for different volume fractions, and the yield stress is smaller than the yield stress of rough particle gels but higher than the one of smooth particle gels. Creep experiments also show that patchy particles behave intermediate between smooth and rough particles, with a "rough-like" behavior for small stresses and the "smooth-like" behavior is for high stresses. This means that while the patchy particles cannot physically interlock, there is still a non-central interparticle force component, which is the source of the increased toughness. However, the fact that the gel is inherently not thermoreversible makes the comparison of its effects a bit more difficult (especially for volume fraction below $\phi = 0.25$), as thixotropy influences the measurement. Nevertheless, this work shows that patchy particles behave half-way between smooth and rough particles, and that the use of patchy particles is an efficient way to increase non-central forces and with that the yield stress, while keeping synthesis efforts low.

Despite lacking precise control over the patch number, shape, and distribution, the synthesis process presented here yields high quantities, facilitating their use in bulk systems like colloidal gels. Rheological analysis reveals intriguing similarities between patchy particles and smooth or rough particles of comparable size. Notably, the plateau modulus of patchy particles aligns closely with smooth and rough particles across varying volume fractions, which suggest that the aggregation mechanism is the same as for homogeneously coated particles. The results point to a universal role of non-central interparticle forces enhancing gel toughness. We highlight the efficiency of patchy particles in increasing non-central forces and therefore the yield stress while minimizing synthesis complexity (for this specific particle system), positioning them as promising materials for diverse applications in colloidal engineering.

2.2 Aspect Ratio and Surface Roughness: Modulating Properties in Colloidal Gels

We synthesized silica rods, using the emulsion based synthesis method previously reported by Kuijk et al. [12]. In this method, rods are formed inside the emulsion droplets that include ethanol, ammonia, water, citric acid and TEOS. The continuous phase is composed of pentanol, and the droplets are stabilized by Polyvinylpyrrolidone (PVP). The mechanism of rod formation is described by Kuijk et al. [12], where the emulsion droplet serves as a reaction vessel. First, the emulsion is formed by adding ethanol, water, sodium citrate and ammonia solution and emulsifying the mixture, where pentanol is the continuous phase. Then, TEOS is added and the mixture is emulsified again, so that it reaches the droplets. The sodium citrate stays at the interface of the droplet and continuous phase and serves as a nucleation site for the sol-gel process of the particle formation. The particle grows towards the center of the droplet, similar to a stalagtite, until the TEOS in the droplet is depleted. This gives the particles a bullet-like shape with a flat base and a pointy tip. The diameter of the droplet is controlled by the size of the droplet, therefore the monodisperisty of the particles will depend on the homogeneity of the emulsion. To that end, different emulsification methods have been investigated by Keyu Yang in the scope of his bachelor's thesis in our laboratory in 2023: bath ultrasonication formed a wide array of different shapes, tip sonication and the use of an ultra turrax homogenizer yielded polydisperse rods. In literature, the emulsion is usually formed by shaking the reaction vessel, and was found to be the most efficient way to form a monodispered emulsion [12]. In this work, we used a bubble tea shaker (Commercial Portable Beverages bubble tea shaking machine, HZ-YYJ-2) to ensure a reproducible shaking motion between the batches.

With this procedure, rods of 4 different aspect ratios (1.5, 5, 9, 11) were synthesized by changing the amount of PVP, ethanol and the temperature. Additionally, round particles were synthesized using the Stöber method. All these particles were also rendered rough using the electrostatic heteroaggregation method [13], where the core particles were first made positive; then smaller (diameter = 25 nm) negatively charged asperity particles were adsorbed to the core particle. All of these particles were coated with an octadecyl

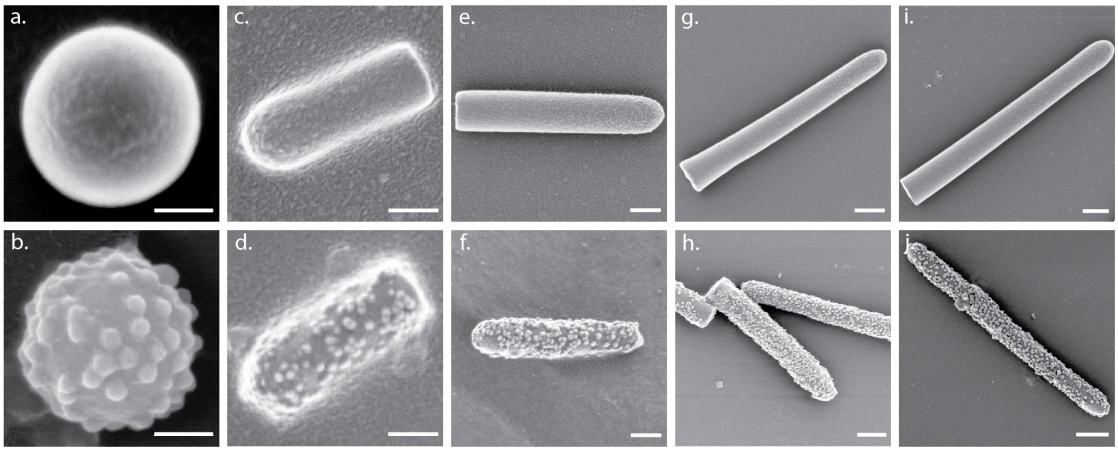

Figure 6: **Silica particles of different aspect ratios with and without surface roughness.** a. AR = 1, smooth, Scale bar = 100 nm; b. AR = 1, rough, Scale bar = 100 nm; c. AR = 1.5, smooth, Scale bar = 200 nm; d. AR = 1.5, rough, Scale bar = 200 nm; e. AR = 5, smooth, Scale bar = 200 nm; f. AR = 5, rough, Scale bar = 200 nm; g. AR = 9, smooth, Scale bar = 400 nm; h. AR = 9, rough, Scale bar = 400 nm; i. AR = 11, smooth, Scale bar = 400 nm; j. AR = 11, rough, Scale bar = 400 nm.

layer using click-like chemistry, so they would form temperature dependent interactions in tetradecane [1]. At higher temperatures, the octadecyl extends into the bulk phase, creating repulsive forces between the particles, and macroscopically behaves like a liquid. At temperatures below 15 °C, the particles become attractive due to an increase in the Hamaker constant and a crystallization of the grafted layer. Figure 6 shows the primary particle samples used in this study, where rough and smooth particles of different aspect ratios were synthesized.

The influence of the particle aspect ratio on the percolation threshold of a geliing systems in a gravitational field was investigated, while comparing the effect of surface roughness to the smooth case. From a rigidity percolation perspective, increasing the aspect ratio adds physical constraints between the particles, eg. at an aspect ratio of 5, the system can be modeled as though 5 spherical particles are attached to form a rigid body. Figure 7 shows that the percolation threshold clearly decreases with increasing aspect ratio, a trend that was previously observed in literature [14]. Further, surface roughness seems to decrease the percolation threshold for lower aspect ratio samples, however the difference decreases as the aspect ratio increases and finally, for an aspect ratio of 11, the percolation thresholds are the same.

The degree of freedom (DOF) of spherical particles is $DOF_{Sphere} = 3$, elongated particles have a higher DOF, as two rotational movements are added to the translational movements, $DOF_{Rod} = 5$. When considering the total DOF of a particle system, we can calculate

$$DOF_{system} = DOF_{particle} * N, \tag{1}$$

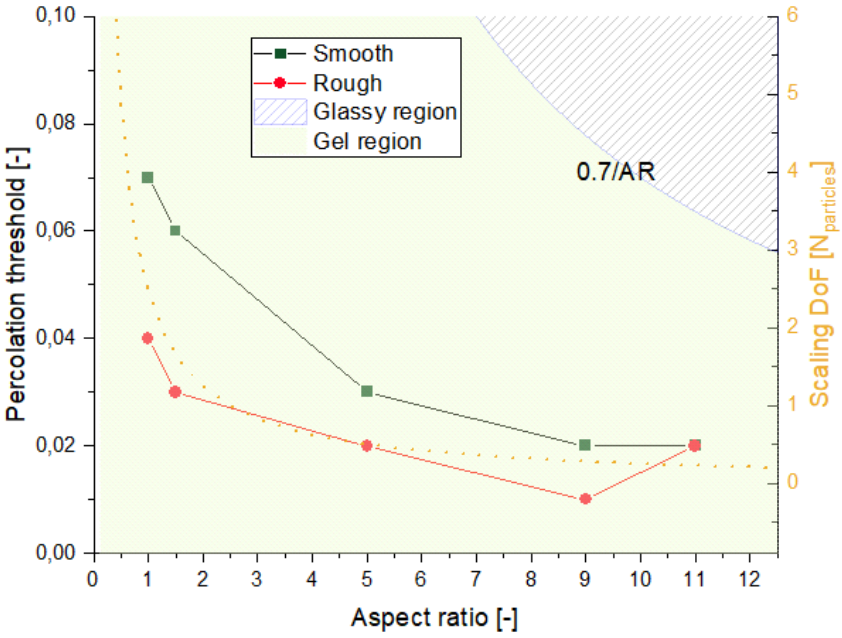

Figure 7: **Percolation threshold of sedimenting and gelling smooth and rough rod-like particles of different aspect ratios.**

where N is the total number of particles. If the total particle volume is kept constant, the total number of particles can be approximated as

$$N(AR) = \frac{V_{tot}}{V_{Sphere} * AR}, \tag{2}$$

where V_{tot} is the total particle volume and V_{Sphere} is the volume of a sphere. Plotting equation 1 in figure 7 shows that the total DOF of the particle system is proportional to the percolation threshold. Intuitively, this translates to rotational hindrance of the particles as the aspect ratio and the dilute limit increases. Additionally, surface roughness influences the percolation threshold similarly to the aspect ratio, in that both inhibit the rotation of the particles. The addition of non-central forces given by surface asperities decreases the rotation and sliding of the particles and so does the aspect ratio, as they get confined in space for lower volume fractions than isotropic particles [15].

A networks microstructure controls the macroscopic elastic and viscous properties. In their extensive review, Solomon and Spicer [15] reduce the rheological behavior of a rod primary particle gel to four physico-chemical properties: (i) interparticle forces; (ii) aspect ratio; (iii) particle number density; and (iv) flexibility. In our system, the rods are rigid, the interparticle forces are constant, but the aspect ratio changes the number density at constant volume fraction as described in equation 2. The elasticity of the gelled structure was investigated through strain amplitude sweeps. For the rough rod gels, the elastic modulus is independent of the aspect ratio, whereas the smooth particle's elastic modulus scales with aspect ratio (see figure 8). This can be rationalized through the increase of the bending stiffness inside the percolated system. The elastic modulus can be calculated as

$$G' = \frac{S}{a} k_0, \tag{3}$$

where S is a constant structure parameter. The effective single bond rigidity

$$k_0 = \frac{12\pi E a_c^4}{a^3}, \tag{4}$$

where E is the Young's modulus, a is the radius of the particle and a_c is the radius of contact [16]. The elastic modulus of both systems show a non-monotonic behavior at low aspect ratios, which has also been observed in simulations. Increasing the aspect ratio increases the area of contact, as the smooth particles tend to form localized isotropic regions. This is not the case for the rough particle system, as the surface roughness hinders the rods to form ordered structures. Therefore, the anisotropic morphology of the gel yields the same structures, independent of the aspect ratio. When considering the geometry dependent contact area between two bodies, two spheres can only touch in one conformation, whereas two cylinders can have a maximal contact area when aligned in parallel and will minimize their contact area when crossing perpendicularly. The geometry dependent central vdW forces between two particles can be calculated for the different conformations, which is directly proportional to the contact area [17]. For two

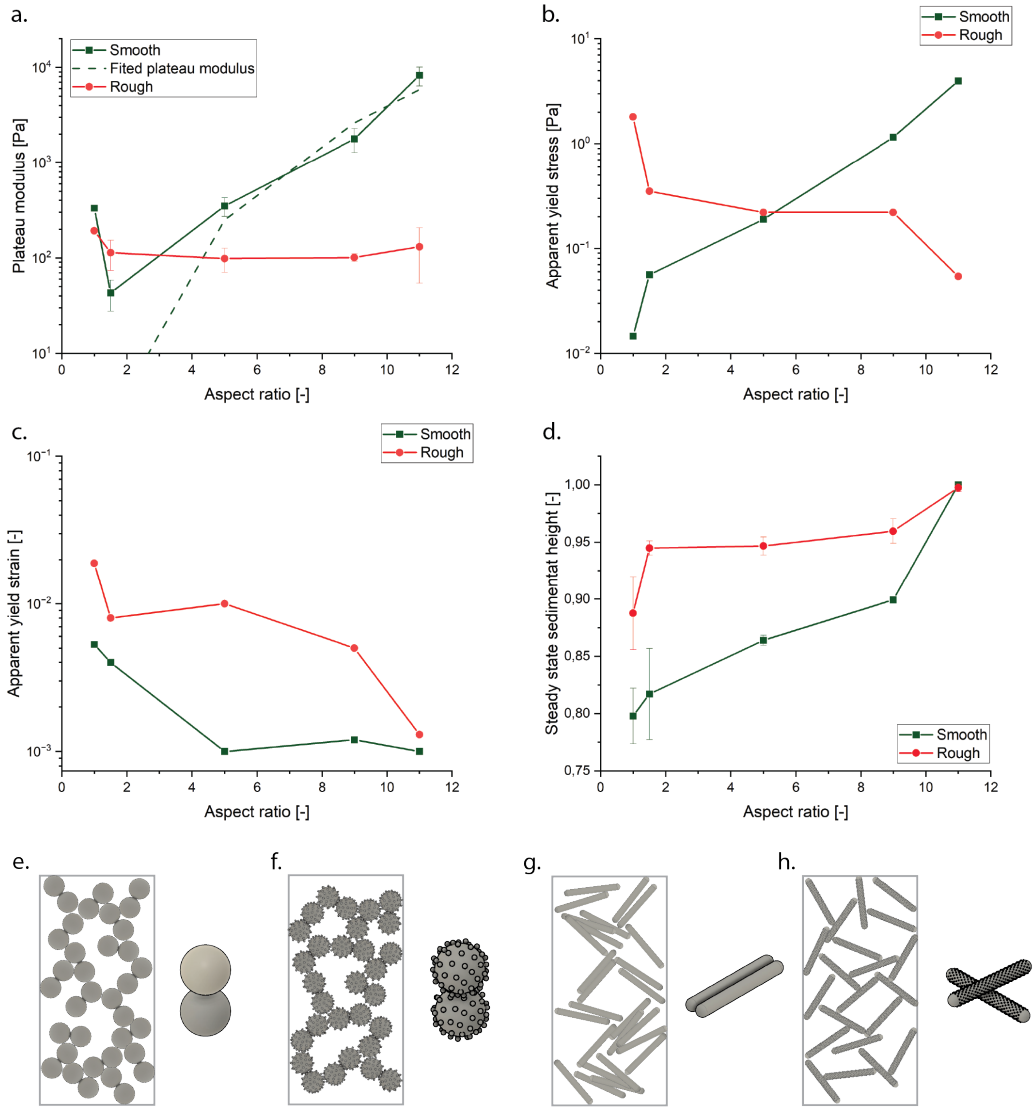

Figure 8: **Rheology and stability characterization of the smooth (green) and rough (red) rod particle gels at volume fraction $\phi = 0.1$**. a. Plateau moduli for different aspect ratios, where the smooth particle plateau modulus is fitted with equation 3, b. Apparent yield stress for different aspect ratios, c. Yield strain at the specific apparent yield stress for different aspect ratios, d. Sedimentation height (h/h_0) for the different aspect ratios, e.-h. Scheme for the particle interactions and network geometry for e. smooth spherical particles, f. rough spherical particles, g. smooth rod particles and h. rough rod particles.

round and smooth particles, $a_c \propto R/12D^2$ (see figure 8e.), for two rough particles, the Rumpf model can be used to take the surface roughness into account: $a_c \propto R/(6(D - D_0)^2(r/(r + R) + 1/(1 - r/D_0)^2$ (see figure 8f.), where r is the radius of the asperity and D_0 is the minimal distance between the two particles (usually 0.3 nm) [18]. When considering elongated particles, the relative orientation of the particle plays a crucial role in the contact area and therefore in the central force. When the rods are aligned perpendicular to each other, $a_c \propto R/D^2$ (see figure 8g.), which will be the prevalent case for rough particles, as the surface roughness will hinder the particles to orient themselves. In the smooth rod systems, however, sliding of the rods after initial contact is possible and more likely to occur, leading to $a_c \propto L\sqrt{R}/D^{5/2}$ (see figure 8h.). The latter relation is the only one, out of the four cases, which is dependent on the length of the particle L. It is important to note, that similarly to the expansion of Rumpf for the contact of rough spherical particles, a similar relation will need to be applied to the overlapping rough rods, which will still be independent of the length. Additionally, inside the gel, the angle between rods will cover the whole range between 0° and 90°, however the elastic modulus data in figure 8a. show clearly, that for the rough system, the modulus is independent of particle length, which is an indication that most of the network is made out of anisotropic particle assemblies.

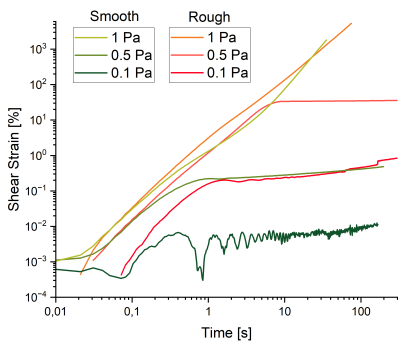

Figure 9: **Creep measurements** for smooth (green) and rough (red) rod gels of aspect ratio 5 at volume fraction $\phi = 0.1$.

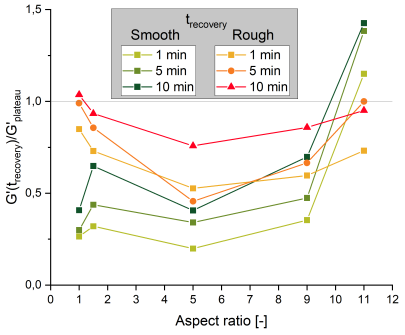

Figure 10: **Recovery measurements** from 100 % strain after 1 min, 5 min and 10 min for gels consisting of smooth (green) rods and rough (red) rods at volume fraction $\phi = 0.1$.

Figures 8b. and c. show the apparent yield stress and strain, respectively, from the oscillatory measurements. For the smooth system, the apparent yield stress increases for increasing aspect ratio [19], while it decreases for the rough system. This can also be explained with increasing bending stiffness in the system, as the yield stress is proportional to the critical moment that a aggregate can sustain [16]. As the bending stiffness increases, so does the critical moment for the smooth rod gels. However in the rough and more homogeneous systems, where the aspect ratio of the primary particles seems

to have less of an influence, the apparent yield stress decreases. Here the particles can interlock, which will give rise to a torque component, more than is possible in the smooth system, as the same kind of forces will induce alignment of the particles through sliding. Figure 8c. shows that the structures become more brittle as the aspect ratio increases, however generally surface roughness makes the structure tougher which has been seen for round primary particle systems [1]. As the rough system is more homogeneous in its microstructure, this explains the increased toughness, while local isotropic regions increase the brittleness. Gravity induced sedimentation subjects particle gels to shear forces, which will cause a change in microstructure. Figure 8d. shows that increasing the aspect ratio of the particles increases the sedimentation stability. Similar to the elastic properties of the rough particle gels, the dependence on the aspect ratio seems to be small. It is only for the AR=11 rough particle gel, that the sedimentation stability is significantly higher than for lower aspect ratios, which might be due to a more homogeneous gel network induced by the increased particle length. For the smooth case, the particle length has a clear influence, which can be related to the bending stiffness that resists the densification of the structure through gravitation.

Shearing elongated primary particle structures induces orientation of the particles, especially in continuous shear experiments such as creep. Figure 9 shows creep experiments for rough and smooth rods at $\phi = 0.1$. At this aspect ratio, the oscillatory apparent yield strains are both around 0.2 Pa. Analogous to the oscillatory experiments, the elastic strain (creep curves at 0.1 Pa) is lower for the smooth than for the rough system. This also means that the elastic region is more narrow for the rough particle system than for the smooth particle system. Generally, however, the fact that the particles can orient in flow direction and the fact that this orientation will be very different in the smooth and rough case because the microstructure is different, makes the comparison of both systems in flow difficult and needs a much more thorough and detailed investigation.

The consequences of shear induced alignment were analyzed through oscillatory recovery measurements, where the sample was sheared at 100 % strain for a minute, before letting the gel recover in the linear elastic region for 10 min. Figure 10 shows the recovery of G' relative to the original plateau modulus of the sample prior to the fluidification. The overview shows that for both rough and smooth rods, the aspect ratio of 5 undergoes a minimum in the ability to recover to the initial structure, which then gets improved with increasing aspect ratio. Interestingly, the smooth rods at an aspect ratio of 11, far overshoot the initial plateau modulus after loading of the sample. This means that the rods must have been aligned by the shear, forming isostatic clusters. As these particles have the longest aspect ratio, an explanation could also be, that a specific relative strain per primary particle length must be achieved in order to align the particle. Previous work on round rough particles showed that adding surface roughness decreases the thixotropic effect of the gel [1]. Here, we see that in the smooth case, aspect ratio seems to decrease thixotropy as well, as long as there is not too much alignment of the particles as this induces large changes in the microstructure. In the rough case, thixotropy is increased for intermediate aspect ratios and decreased again for aspect ratios 9 and 11, but in

general, rough rod systems are less thixotropic than smooth rod systems.

Rheological properties already hinted at microstructural differences between the rough and the smooth system. In this section, the microstructure was analyzed through confocal microscopy, by labeling the rods fluorescently. A rough and smooth gel ($\phi = 0.1$) of AR=11 rods was formed in a rectangular cuvette, and left to sediment for 11 days, the microstructure was then imaged at 4 different points along the height of the cuvette, namely the bottom, 1/3 of the length, 2/3 of the length and the top of the cuvette. As the particles at the bottom of the vial are exposed to more shear than the particles on the top, this leads to a gradient in shear forces, that is recognizable in the images after 11 days of sedimentation. The images show that, indeed the smooth particle system seems to have local isostatic ordering (see figures 11e.-h.), while the rough particle system is mostly homogeneous throughout the imaging field (see figures 11a.-d.). There is also a trend of densification in the rough particle system on the bottom of the vial, which is apparent through some denser clusters. The smooth particles seem to densify less on the bottom of the vial, the isostatic clusters are lager on the bottom than on the top of the vial, which could indicate densification, but the volume fraction does not seem higher on the bottom than on the top. To make the comparison of the different systems more quantitative, different image analysis approaches were attempted. Due to the small size of the particles and the dense clusters, it was not possible to segment single particles [20]. Therefore, the Moran's Index was computed, which is a pixel based analysis that does not require the detection of single particles. In a binary image, the local Moran's I is calculated for every pixel in the image and will be 1 for highest spatial autocorrelation and 0 for no spacial correlation. Figure 11i. shows averaged Moran's Index, where the homogeneous nature of the network of rough rods generally shows a more correlated image than the images of smooth rods. The optical data suggest that the mechanisms that prevent sedimentation are different in both systems. In the smooth particle gel, an increased bending stiffness might arise from the localized isotropic regions, whereas a homogeneous wide spanning network of interlocked particles is responsible for the stability of the network in the case of the rough particle gels.

Aspect ratio of the constituent particles is a powerful parameter to engineer colloidal gels. For smooth particles, increasing aspect ratio increases elasticity, the apparent yield stress as well as the stability to sedimentation increases while mitigating thixotropic effects. The fact that elongated systems can orient and form local isostatic clusters increases the bending stiffness inside the network, which is responsible for the above mentioned properties. Moreover, when sliding and aligning of the particles is hindered through surface roughness, the network structure is more homogeneous and anisotropic, which decreases the effect of aspect ratio on properties such as elastic modulus, sedimentation properties and shear recovery. This difference in microstructure was also shown in confocal images. Increasing aspect ratio lowers the dilute limit at which the particles can interact, as their hydrodynamic radius will increase. This decreases the percolation threshold in a similar way for rough and smooth rods, as the difference in the surface occurs mainly when particles are in contact.

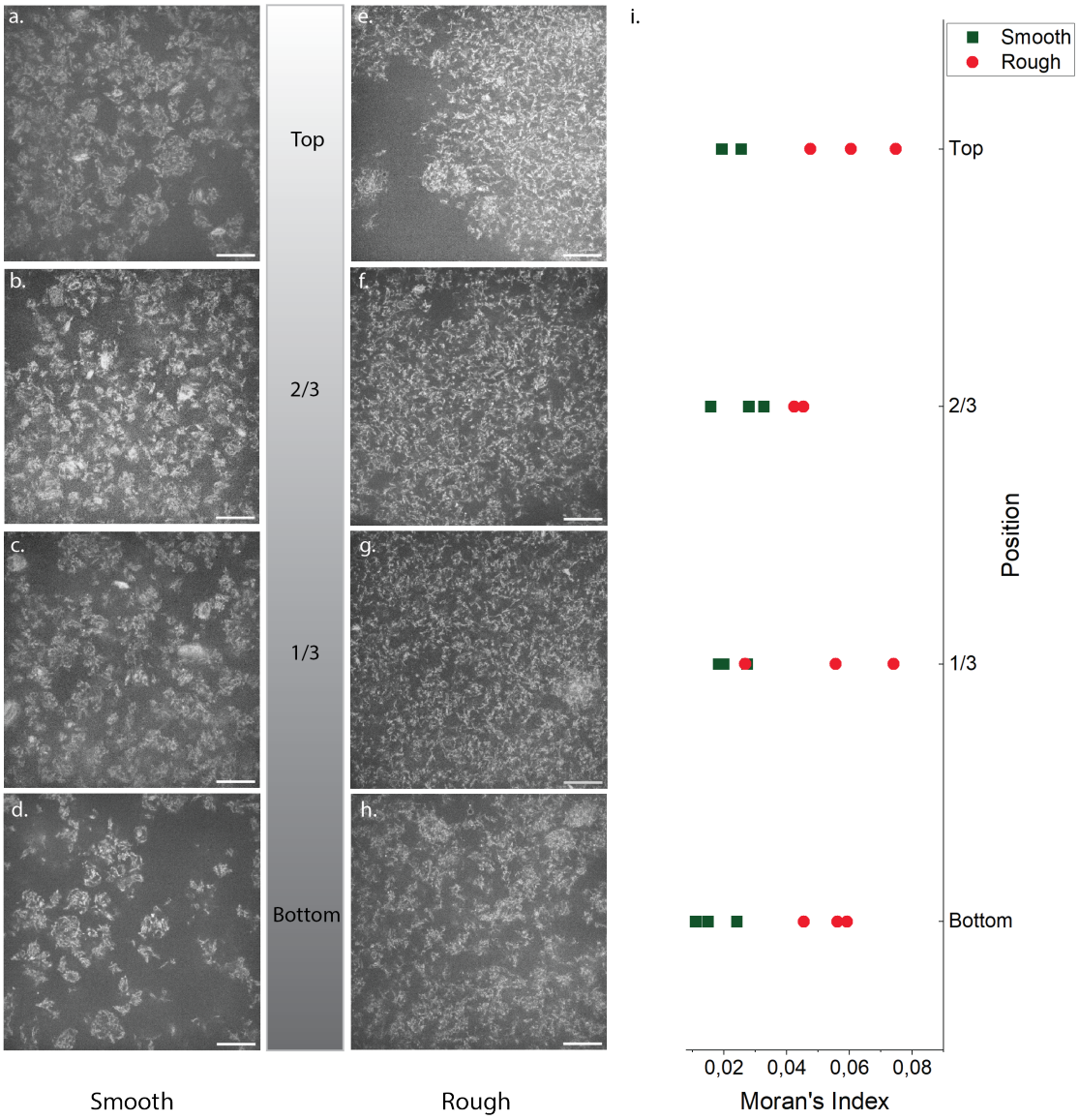

Figure 11: **Sedimentation of AR=11 rod gels at a volume fraction $\phi = 0.1$ after 11 days of sedimentation.** a. Smooth rods at the top of the cuvette, b. Smooth rods at 2/3 from the bottom of the cuvette, c. Smooth rods at 1/3 from the bottom of the cuvette, d. Smooth rods at the bottom of the cuvette, e. Rough rods at the top of the cuvette, f. Rough rods at 2/3 from the bottom of the cuvette, g. Rough rods at 1/3 from the bottom of the cuvette, h. Rough rods at the bottom of the cuvette, i. Averaged Moran's Index for the rough and smooth system at the different positions.

The aspect ratio of the colloidal building blocks plays a crucial role in the engineering of colloidal gels, impacting various properties such as elasticity, yield stress, gravitational stability, and thixotropic effects. Increasing aspect ratio lowers the threshold of the dilute concentration regime, ands the percolation threshold becomes independent of surface topography. Smooth particles with higher aspect ratios display and enhanced elasticity and stability against sedimentation, attributed to the formation of local isostatic clusters within elongated systems, thereby increasing network stiffness. The addition of surface roughness to elongated particles, which inhibits sliding and alignment, resulting in a more homogeneous and anisotropic network structure, mitigating the aspect ratio's effect on properties like elastic modulus, sedimentation behavior and shear recovery.

3 Describing plasticity in soft solids: from microscopic visualization to macroscopic modeling

3.1 First characterizations of plastic events in a slowly sheared weak depletion gel

One of today's challenges pursued in the soft solids community is to provide direct imaging of colloidal gels under shear at a time resolution enabling the observation of rare events at the origin of their yielding [21]. These events consist in rearrangements of particles triggered by a relaxation of localized stress during mechanical loading. [22] These studies should also enable us to link subtle changes in physical chemistry influence gel mechanics, by understanding their effects on the fundamental plastic events. Studying these latter and their properties are crucial in order to elaborate microstructure-based models which can predict the macroscopic response of the soft material, or to highlight physico-chemical knobs that can be used to control plasticity in the structure of the material [2].

After emphasizing in the previous reports the post-processing of raw experimental data from our ultrafast rheo-confocal setup leading to time-resolved 3D reconstructions of partial colloidal gels structure showing plastic events, we present in this section a more detailed characterization of these events occurring in a weak depletion gel of PMMA-g-PHSA particles, known as a model material suited for rheo-confocal studies. More especially, we focus on the effects of volume fraction and attraction strength between the colloidal particles in the gel on the size of these plastic zones and the rate at which they appear, for larger observation windows as previously done.

A first characterisation of the bulk rheological properties of the system at different volume fraction and interaction strength is carried out. After erasing the shear history of the sample through a pre-shear step at Pe = 20 and a recovery of 5 minutes, the depletion gel undergoes an amplitude sweep. Snapshots of the structure after the pre-shear and recovery in Figure 12 seem to correlate with the evolution of the plateaus of G' and G" in the linear regime. [23] Indeed, they increase with increasing volume fraction

[2] This is the work of graduate student Pierre Lehericey, who will graduate towards the end of 2024

and interaction strength and the dynamic yield stress is around 1%. Nevertheless, it has to be noted that the gels are, as expected, very weak with a maximum storage modulus of around 10 Pa. The rheological measurements are then very close to the detection limit of the rheometer represented by the low torque limit superimposed on all graphs in Figure 12 (b), or even below for the lowest volume fraction and the lowest interaction strength. In this case, the formation of a gel could have been confirmed by the absence of Brownian motion of the particles after gelation.

After confirming the formation of a gel, we can now perform experiments that are the most likely to trigger the formation of plastic events. The two methods chosen are strain-controlled flow reversals and stress-controlled creep. In this report, we will emphasize on flow reversals reaching a strain of 1% at a strain rate of 1.10^{-3} s^{-1}. During this mechanical solicitation, the structure is monitored using **optical flow with a pyramidal Lukas-Kanade method** which enables a good compromise between precision and robustness for the detection of discontinuities in the materials flow while being nearly insensitive to the complex background of the confocal 3D stacks. The obtained heat maps of Figure 13 reveal the presence of plastic zones of particles rearrangement even at low deformations in the elastic regime of the material.

This is reminiscent of what Cipeletti et al. depicts as "precursors of failure". [24] Correlation with the local strain field obtained from finite strain theory shown in Figure 14 can be achieved. The size of the plastic zones obtained by optical flow seem to correlate with the size of the variation of the local strain field at the same position and at the same time. For any case, this size is always smaller than the one observed for similar materials like colloidal glasses. This is a consequence of the less particles-crowded structure of the gel as well as the presence of interactions that limit the degree of freedom of particles that could rearrange in colloidal glasses just by thermal fluctuations. [25]

The two physico-chemical parameters varied here, namely volume fraction and interaction strength between particles, have an important effect on the aspect of the local strain map. Indeed, as summarized in Figure 15, not only the size but also the rate at which plastic rearrangements happen decreases with increasing volume fraction and interaction strength, in a monotoneous fashion. At the low shear strain reached and at the slow shear rate of the experiment, it is possible to imagine that the mechanical energy given to the system is enough to trigger some rearrangements only in systems where the activation barrier is small enough, which can correspond to low interaction strength systems and open systems in which particles have more free space to rearrange.

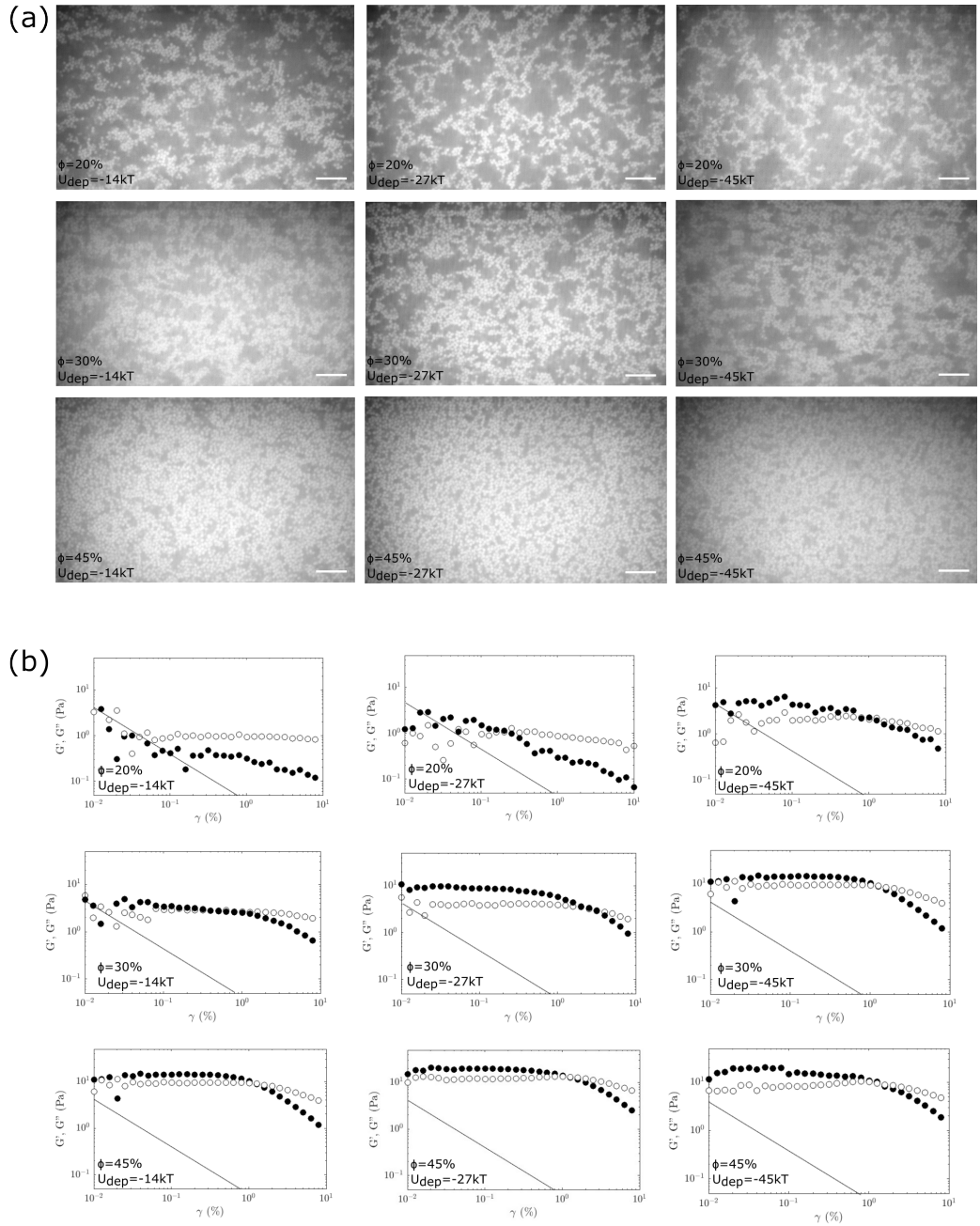

Figure 12: Structure (a) and amplitude sweeps (b) obtained with the rheoconfocal setup of PMMA-g-PHSA depletion system at various volume fractions and interaction strength. The white scale bar in (a) refers to 10 μm. In (b), filled circles correspond to G', empty circles to G" and the black line corresponds to the low torque limit of the instrument

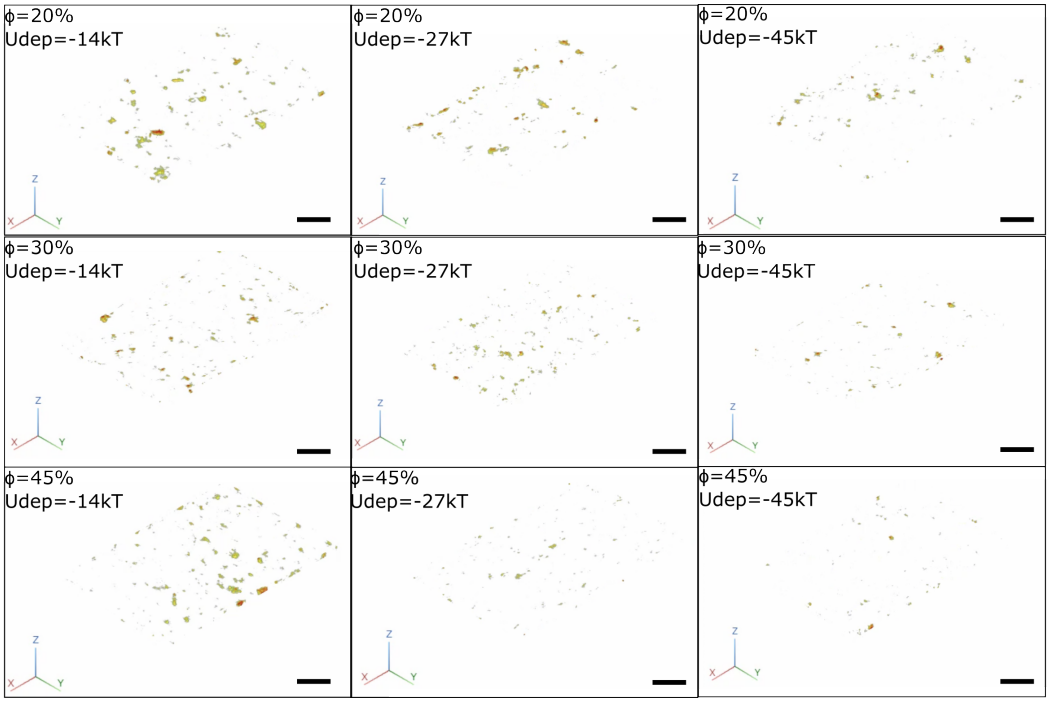

Figure 13: Heat zones of plastic activity obtained by optical flow with the pyramidal Lukas-Kanade method during a flow reversal experiment. The black scale bar refers to 10 μm

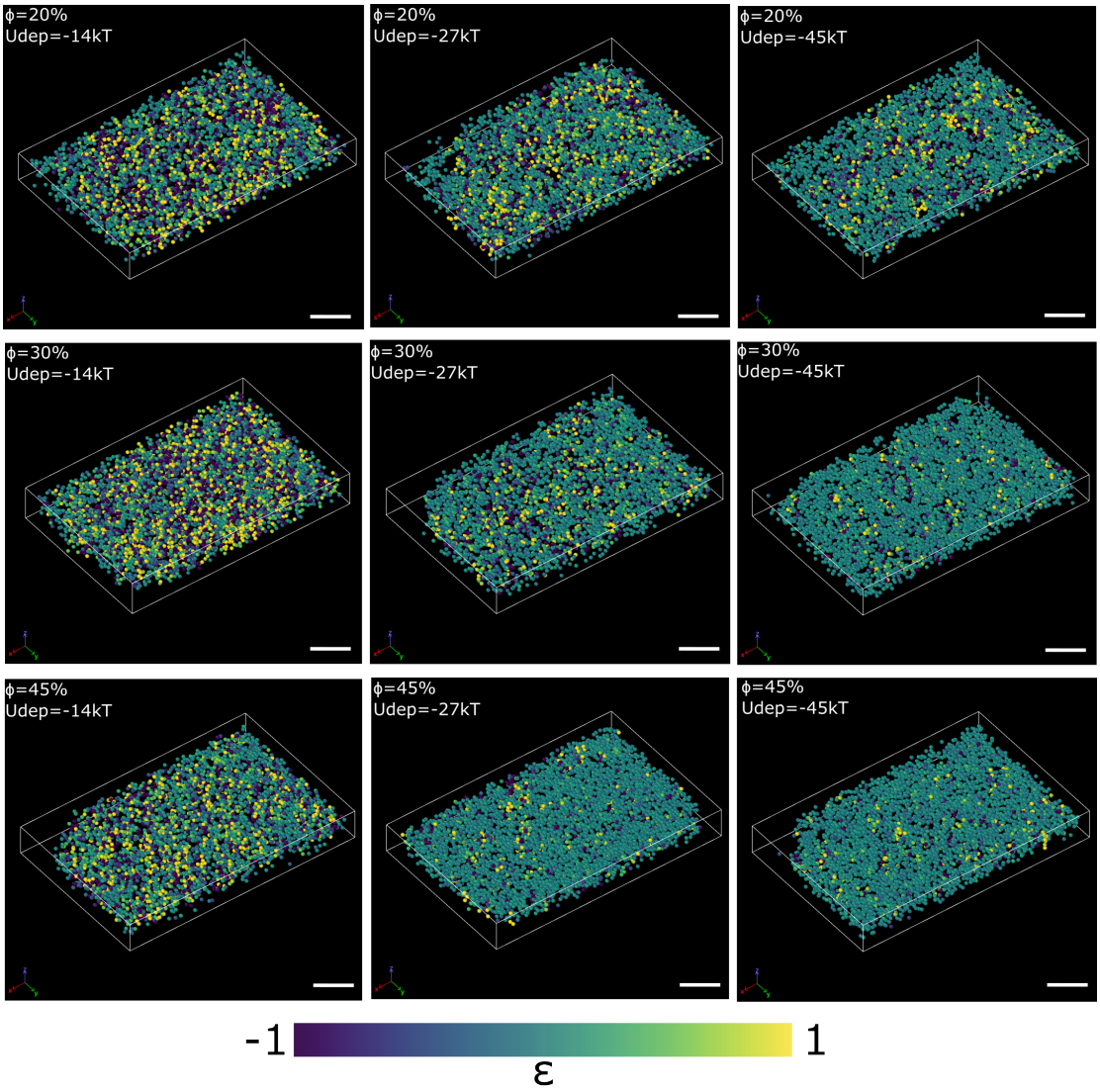

Figure 14: Reconstructions obtained by particle tracking of gel sections undergoing flow reversal at different volume fractions and interaction strength. Particles are color-coded according to their local strain. White scale bar refers to 10 μm

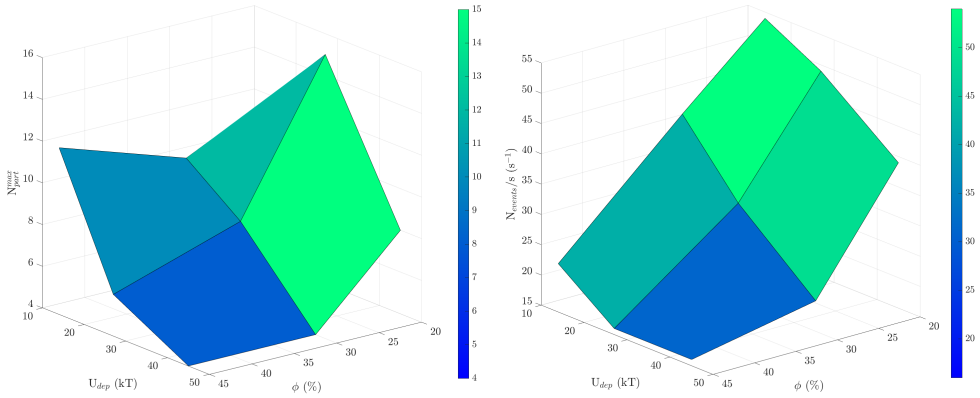

Figure 15: Evolution of the number of particles in the rearrangement zone (left) and of the rate of plastic events in the structure (right) as a function of depletion potential and volume fraction

Visualization of plasticity in colloidal gels is achieved here by analysing rheo-confocal data with a combination of so called optical flow and particle tracking techniques. These latter emphasize the role of volume fraction and interaction strength on the characteristics of plastic events and, in the end, on the stability of the colloidal structure. Further analysis on flow reversals varying the shear strain and the shear rate, as well as on creep experiments is ongoing in order to give the most complete picture of plastic rearrangements possible. This method will soon be applied to the thermo-reversible systems depicted in Section 2.

3.2 Advancement in modelling yield-stress material: multi-mode description and tensorial model

Understanding the mechanical behavior of soft solids is crucial across various fields, from materials science to bio-mechanics. At the heart of this lies constitutive modeling, which provides a framework to describe how these materials deform under different loading conditions. Building upon our previously established model [26][3], we now aim to extend its capabilities to encompass a broader range of deformation modes and realistic materials, thereby offering a more comprehensive representation of the complex behavior exhibited by soft solids.

The first of these extension is the multi-mode formulation of the shear model, which use a broader distribution of relaxation times instead of a single time to model a 0.5% Carbopol dispersion. To achieve this the relaxation spectrum can be either approximated by a number of separate Maxwell modes or captured by a suitable functional form of the linear shear-relaxation modulus [27–29]. To implement the second method, the model has to be converted to an integral formulation, as expressed in Eq.(5d-6c). Where $G(t)$

[3] work of Graduate student Gabriele Pagani

is the linear shear-relaxation modulus and ψ is the so-called "reduced time". The lower bound of the integrations $t'' = -\infty$ indicates that all previous deformation history has to be taken into account. If the sample are conditioned before deformation, as done in our experiments, the integrations run from $t'' = 0$. The last equation, Eq. (6c), is the material shift-factor expressing the stress dependence of the material. In our case was found that a Ree-Eyring type shift-factor was optimal to describe the non-linear behaviour observed. The non-linearity is given by two relaxation mechanism, each of them with a characteristic stress $(\sigma_{01}, \sigma_{02})$ and a characteristic viscosity (η_{01}, η_{02}). The function is normalized by the zero-shear viscosity η_0.

$$\sigma(t) = \int_{-\infty}^{t} G\left(\psi - \psi'\right) \dot{\gamma}\left(t'\right)\, dt' \tag{5a}$$

$$\psi = \int_{-\infty}^{t} \frac{dt''}{a_\sigma\left(\sigma(t)\right)} \tag{5b}$$

$$\psi' = \int_{-\infty}^{t'} \frac{dt''}{a_\sigma\left(\sigma(t)\right)} \tag{5c}$$

$$a_\sigma(\sigma) = \frac{\eta_{01}}{\eta_0} \frac{\left(\frac{\sigma}{\sigma_{01}}\right)}{\sinh\left(\frac{\sigma}{\sigma_{01}}\right)} + \frac{\eta_{02}}{\eta_0} \frac{\left(\frac{\sigma}{\sigma_{02}}\right)}{\sinh\left(\frac{\sigma}{\sigma_{02}}\right)} \tag{5d}$$

The linear modulus was approximated by the fractional Maxwell-liquid model, that through the use of a "spring-pot" element express an hybrid behaviour between a purely elastic response and a purely viscous response [30, 31]. The fractional model is parameterized on the linear compliance data, obtained by the shifting to zero stress of the compliance data at 20 Pa, Fig. 16a. The shifting was carried out according to the stress-time superposition, demonstrated in Pagani et al. [26]. The model used has the additional advantage that the creep compliance, Eq.(6a), could be analytically inverted in a relaxation modulus, Eq.(6b-6c).

$$J(t) = \frac{t}{\eta_0} + \frac{1}{\mathbb{G}} \frac{t^\beta}{\Gamma(1+\beta)} \tag{6a}$$

$$G(t) = \mathbb{G} t^\beta E_{1-\beta,1-\beta}\left(-\frac{\mathbb{G}}{\eta_0} t^{1-\beta}\right) \tag{6b}$$

$$E_{a,b}(z) = \sum_{k=0}^{\infty} \frac{z^k}{\Gamma(ak+b)} \tag{6c}$$

Once a suitable form of the linear modulus was achieved, it was employed in the integral formulation of out model, Eq.(5). This could let us refine the prediction of transient

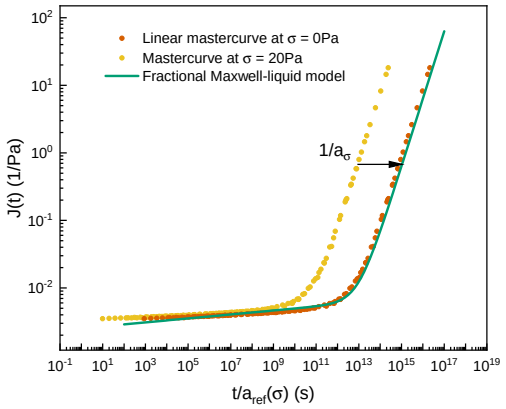

(a) **Compiance mastercurve** obtained by data (yellow dots), its shifting to the linear response (orange dots) and fitting with the fractional Maxwell-liquid model (green line).

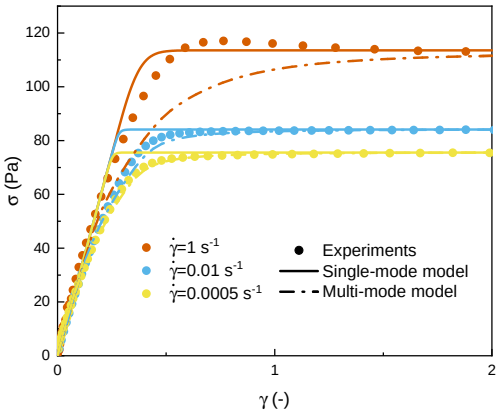

(b) **Start-up** measurements (dots) and model predictions. Continuous lines are the single relaxation time model predictions, while the dash-dot lines are the predictions of the multi-mode model.

Figure 16: Parametrization and predictions of the **multi-mode shear model**

responses, as shown in Fig. 16b for start-up experiment. The predictions of the multi-mode model closely align with experimental results, especially at low shear rate where plastic deformation is more important and our assumption are more relevant. The predictions offer a smoother transition compared to the single relaxation time model, enhancing its accuracy.

The initial shear model could also be generalized in order to describe multi-directional deformations using a tensorial description. For incompressible material, the obtained model is presented in Eq.(7) and it was firstly derived by Tervoort et al. [27, 32] for glassy polymers. The following model was proved as thermodynamically admissible and objective by deriving this class of elastoviscoplastic constitutive relation with the GENERIC formalism [33, 34]. The subscripts e, p and eq, respectively, means "elastic", "plastic" , and "equivalent" nature of the quantity of interest, while the superscript d indicate the deviatoric part of a tensor. The material derivative is represented by the symbol D_t, the left Cauchy-Green strain tensor by $\boldsymbol{B}$, and the strain rate tensor by $\boldsymbol{L}$

$$\boldsymbol{\sigma}^d = G\boldsymbol{B}_e^d \tag{7a}$$

$$D_t\left(\boldsymbol{B}_e\right) = \left(\boldsymbol{L} - \boldsymbol{L}_p\right)\cdot\boldsymbol{B}_e + \boldsymbol{B}_e\cdot\left(\boldsymbol{L} - \boldsymbol{L}_p\right) \tag{7b}$$

$$\sigma_{eq} = \sqrt{\frac{1}{2}\boldsymbol{\sigma}^d : \boldsymbol{\sigma}^d} \tag{7c}$$

$$\boldsymbol{L}_p = \frac{\boldsymbol{\sigma}^d}{2\eta\left(\sigma_{eq}\right)} \tag{7d}$$

$$\eta\left(\sigma_{eq}\right) = \eta_0 a_\sigma\left(\sigma_{eq}\right) \tag{7e}$$

The elastic strain defines the stress perceived by the material, Eq.(7a), where the two quantities are directly proportional through the shear modulus G. The accumulated elastic strain is relaxed by the plastic deformation rate $\left(\boldsymbol{L}_p\right)$ as expressed in Eq.(7b), this relation transform in a simple summation of elastic and plastic shear rate in the case of simple shear. The model can be used to predict very complex deformations, e.g. entrance flow. However, it should be validated on homogeneous deformation to clearly reconstruct the different components of the stress and strain tensors. Simple shear and uniaxial-compression were chosen as characteristic deformation protocols due to their simplicity and relevance. The shear measurements are the standards for colloidal suspensions, and for a tensorial study they should be enriched by normal force measurements that express mechanical cross effects, this measurements are encountered less often but can be found abundantly in the literature. Instead, uni-axial compression are difficult to perform and therefore not prominent in soft pastes literature. for this reason the results obtained would be presented in their own chapter.

The shear model reported in Pagani et al. [26] is extended to predict more realistic materials and deformations. Multiple relaxation times, fingerprint of complex fluids, are approximated through a linear shear-relaxation modulus, then used in the integral form of the shear model. The relaxation modulus was calculated from the fractional Maxwell model fitting of the linear compliance. The tensorial generalization of the shear model is proposed here to extend the validity of it to deformations that industrial samples could experience in their lifespan, in particular for two relevant cases (simple shear and uni-axial compression). The stress activation function connects the macroscopic modelling with the microscopic world and gives a new way to think about formulations. We also started applying this model to the industrial dispersions.

3.3 Uni-axial compression for soft pastes

As explained before, uni-axial compression measurements are theoretically a simple experimental protocol, given the homogeneity of the deformation and the small amount of tensorial component involved, but they result difficult to perform in laboratory practice when soft solids are under study. The complexity of these experiments derive from the ill controlled boundary between the material and the geometry. Often pastes adhere to the flat geometry generating a no-slip condition, or partially slip condition, during the experiment. This cause the sample to take a characteristic barrel shape and break the homogeneity of the deformation [35, 36]. To avoid this, a special coating was developed specifically for the material used (Carbopol 940) that repel the microgel particles, forming a depletion layer that effectively lubricate the material assuring a total slip boundary condition. It was then possible to perform clear compression measurements for dispersion of different concentration, in particular two weight concentrations were used, 1% and 0.15%. These test the model at its limits and they highlight the reliabil-

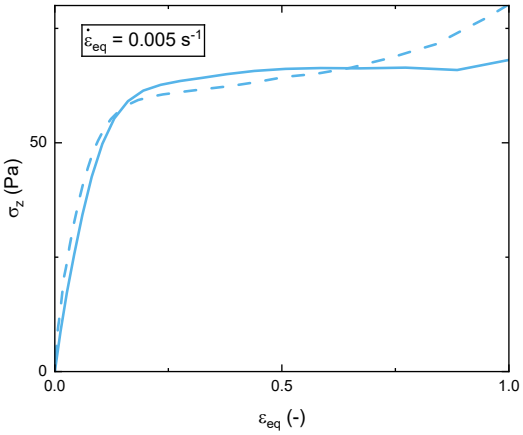

Figure 17: Repetition of a uni-axial compression with a constant equivalent strain rate of 0.005 s^{-1} for a 0.15% dispersion of Carbopol 940. The two curve show good reproducibility until $\epsilon_{eq} = 0$. After that is is possible to observe a deviation of the dashed line that is characteristic of lubricant loss.

ity of the measurement protocol. Indeed, a repetition of compression with a constant Hencky strain-rate is presented in Fig. 17, showing the good reliability of the performed measurements.

Carbopol dispersion are considered to be typical simple yield-stress material, so during constant strain-rate deformation they are expected to show a simple plastic response, with a the constant stress after plastic yielding. The shear data, presented in Pagani et al. [26], show exactly this behaviour with a minimal overshoot for fast deformation. The uniaxial compression measurements could be more complicated, showing strain-hardening for dispersions with high concentration. The results for the 1% dispersion are reported in Fig. 18a with also the model prediction. Even if strain-hardening is not explicitly considered in the model, the stress plateau value predicted agree with the yield-point extracted from the strain-hardening curve, showing the capability of the model to capture the salient aspects of soft pastes. From a microstructural point of view, the strain-hardening is given by the deformation, and subsequent anisotropy, of the microgels during compression.

For low concentration of microgels the material show a clear simple plastic behaviour during compression. As much as the overall behaviour is the one expected by the model, its predictions result lower than the measured value, as presented in Fig. 18b for the 0.15% dispersion. The offset can be explained by the failing of the Von-Mises criterion for yielding, used in the model to calculate the equivalent stress, and so a concentration dependency of the yield rule that should employed by the model.

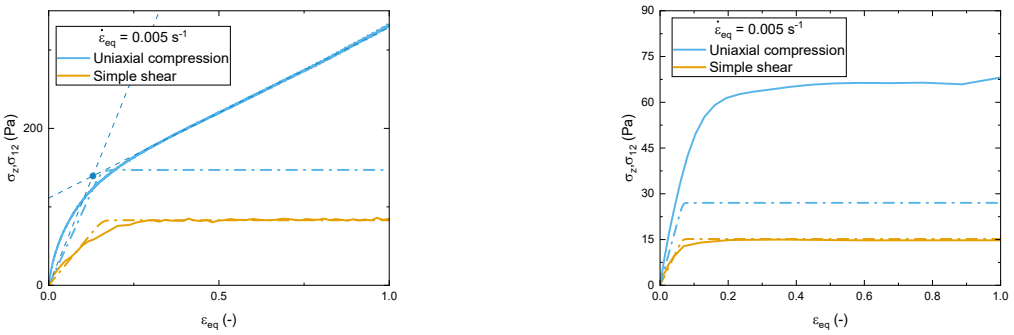

(a) 1% dispersion

(b) 0.15% dispersion

Figure 18: Uni-axial compression with a constant equivalent strain rate of 0.005 s^{-1} for two concentration of Carbopol: (a) 1% and (b) 0.15%. Dash-dot lines represent the model prediction while the continuous lines are the experimental data. The two dashed lines and the dot in (a) represent the yield-point construction for strain-hardening samples.

The simplicity of compression is hindered for soft materials by the poor control on the boundary conditions. Uni-axial compression experiments were performed on soft pastes at different concentrations while controlling the slip of the material with the geometry. We observe a concentration dependence on the material response during compression, from strain-hardening for highly constrained particles to simple plastic deformation for samples closer to the jamming volume fraction. The results were analysed in light of the developed constitutive model.

3.4 Sedimentation of industrial dispersions

The final aim of the model is to be used to predict slow deformations in real situations. As a first application, we are pairing with Syngenta to tackle the prediction of sedimentation of flocculated system over long time. The idea is to use a simple set of experiments to recover the model parameters and use them to predict the long term mechanical response.However, flocculated gels are microstructurally significantly different than soft pastes, where the microstructure has not restructuring and therefore thixotropy is absent. This leave our model only as a simplification of the real plastic behaviour of flocculated materials, reducing its capability. To re-extend them a neural network is employed as a mechanical model for sedimentation, bypassing the fine consideration that are needed to capture the sedimentation of flocculated system analytically or numerically. The experimental set chosen is a single flow-curve and and an amplitude sweep, these indeed are the minimal amount of data necessary to parametrize the model. In particularly a PINN (physical informed neural network) will be use, where a simplified model is added to guide the minimization of the neural network. Indeed, the same simplified model

would be used to generate the object of the minimization. At this moment the work is focusing in the definition of a simplified sedimentation model that is able to capture the salient feature of sedimentation without a quantitative prediction of them.

4 Optical tweezer: Insights into the building blocks of colloidal gels

The rheological properties of soft materials, such as colloidal suspensions, gels, foams, or biological matter, have long been the focus of scientific inquiry. Macroscopically, these materials are well understood using characterization methods such as rheology. Colloidal gels and their structural properties can be analyzed from both macroscopic and microscopic perspectives. At the microscopic level, these gels are composed of individual colloidal particles, while at a larger scale, they can be viewed as clusters of these particles. Understanding the formation of these clusters and how their rigidity is affected by the interactions between individual particles is crucial for comprehending the overall rheological characteristics of the gel. This knowledge provides insights into how to deliberately engineer colloidal gel structures with specific rheological properties.
Single particle-particle interactions can also be investigated using methods such as an atomic force microscope (AFM), particle tracking (passive microrheology), or magnetic tweezers. Here, we[4] use an optical tweezer (OT) - a cutting-edge tool that circumvents many restrictions of the above-mentioned techniques. The OT exerts radiation pressure on dielectric particles with a focused laser beam, enabling precise manipulation at the microscale. The forces exerted by an OT can rival those arising from temperature fluctuations and viscous forces, making it a fascinating tool for studying micromechanical structures and mechanisms. Compared to passive microrheology, the forces generated allow for direct oscillatory measurement with higher forces and spatial control of the probe. Compared to magnetic tweezers, the forces that they can exude are two orders of magnitude smaller than in an OT setup. However, their advantage lies in the ability to manipulate a probe with pinpointing accuracy. This advantage makes OTs ideal for studying complex samples with heterogeneous structures [37].

4.1 Bending of linear aggregates

When time-shared traps are used, silica microparticles can be assembled into a linear aggregate of particles [38] By having multiple traps in a line, with colloidal particles trapped inside each trap, and then reducing the distance of the trap position, the particle from a linear aggregate through the particle-particle interaction potential.
In the next step, the aggregated particles can be held only by three traps: two at the chain end and one in the center particle. A bending moment can be induced on the linear aggregate by perpendicularly moving the trap in the center of the chain. The bending force can be obtained from the displacement of the end particles compared to the optical particle positions held in place. [39]

[4]Work of graduate student Lukas Woolley, with the help of Prof Eric Furst, University of Delaware

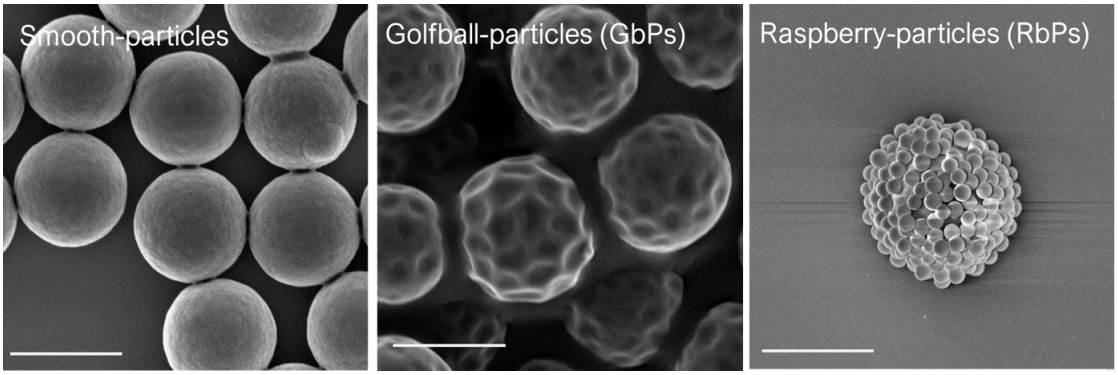

Figure 19: A. Smooth particles, GbPs and RbPs, SEM graphs at 4 kV and 30'000 x magnification; scale bar corresponds to 2 µm.

The first experiments will be a recreation of the bending stiffness work of Furst and Patina with smooth silica particles coated with MPTMs ((3-Mercaptopropyl)trimethoxysilan) [38] 19 a., to confirm that bending experiments are possible with our set-up and our model particles. Afterwards, different non-spherical particles will be tested with the same protocol. In particular, particles with concave and convex asperities on the otherwise smooth surfaces, which we call Golfball-like [40] and Raspberry-like particles [13].

These experiments aim to assess the role of roughness in bending mechanics and explain how non-central forces induced by roughness can affect the bending modulus and bending behavior of linear aggregates. This bending modulus can then be used to describe the mechanical properties of gel structures on a macroscopic level through a constitutive equation. The behavior could also differ depending on what kind of failure mode (sliding between the particles) occurs. By understanding these forces on both micro and macro levels, the desired properties of these structures can be engineered. A better understanding of this mechanism will help us achieve this goal.

4.2 Micro-machines operated by an optical tweezer

The operating range of the OT can be expanded to include integrated micro-machines, such as micro-levers. These micro-levers can multiply the forces applied onto a sample and enable the examination of samples with refractive indices similar to those of the surrounding media and radiation-sensitive samples, which can be the case for biological samples. As demonstrated in previous studies [41], Lever-building techniques have produced micro-levers that can be "slapped" onto samples, allowing for the investigation of resonance and other mechanical properties. These micro-machines can be manufactured using two-photon lithography techniques.

This novel approach holds promise in advancing our understanding of the complex dynamics of particles at interfaces and their response to external forces. Using the same

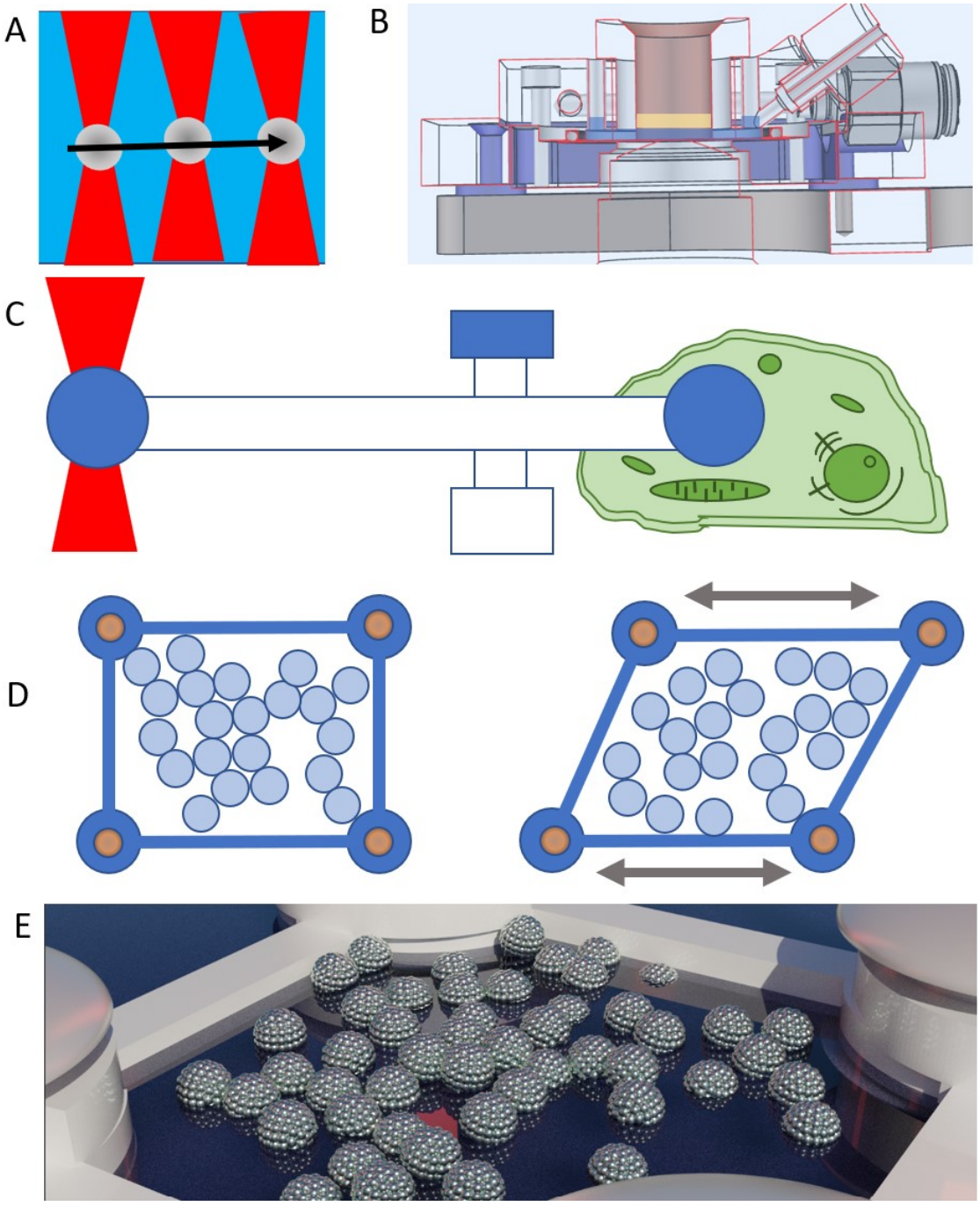

Figure 20: A. Multiple traps in the same microscope set-up, B. Observing cell, allowing the study of liquid-liquid interfaces very close to the glass slide so that an optical tweezer can be employed C. A micro lever for studying samples from a distance and having a stronger force. D. The same principle of the lever can be used to make freely movable joints, which can be employed at a liquid-liquid interface to study different configurations of particles and how they respond to shear deformation. E. A 3d rendering of the situation explained in D.

principle as for the microlevers, joints could be formed. And four of those joints could form a shearable rectangle. The working principle is shown in 20 D. from a top view of the liquid-liquid interface, with some in synchronicity moving traps located at the structure's joints, shear deformation could be induced inside of the rectangular structure. Multiple particles could be placed inside the structure in different configurations. Allowing for the testing of different configurations of aggregates of particles under shear deformation further elevates our understanding of particles trapped at the interface and what influences the mechanical properties of a Pickering emulsion. Recent computational work [42, 43] revealed that in gel network structures, some particles in the network are more integral for the stress-bearing of said network structure than others, to see whether this can also be done in an experimental setup. The set of possible movements, like bending, twisting, and translational movement, can be restricted through either geometrical means or through interaction forces between the particles. In order to measure the impact of the role of single particles on aggregates in isostatic conditions, we aim to determine how removing particles affects the shear modulus of individual aggregates. To achieve this, we plan to use multiple traps to confine the particles and then assemble them to aggregates. Afterward, the shear measurements should give us some insight into the role of single particles on the cluster's mechanical properties. For this to work, several prerequisites have to be fulfilled.
First, the optical tweezer set-up must be capable of moving multiple traps simultaneously 20 A. Secondly, a liquid-liquid interface has to be close to the glass slide so that the laser can be focused on the interface 20 B. (The radiation pressure force scales with the numerical aperture of the objective). The lever principle must be tested, and the assembly procedure must be well understood before going to the free-moving joints. Figures 20 C. 20 E. shows an artist's interpretation of the situation in a 3D rendering.

We have constructued an optical tweezer to interrogate the micromechanics which lead to a stiffening of the nodes in colloidal gels

5 Conclusions

1. Effects of Particle roughness, shape and patchiness have been studied. The data showed how noncentral forces act as tools for tailoring gel rheology
2. A full study of the structural evolution of plastic events by 4D Confocal rheology is underway.
3. A minimal rheological model for elastoplastic materials have been further developed. It builds in understanding how plasticity is stress activated.
4. An optical tweezer setup has been built to understand the link between plasticity and physcial chemistry.

References

[1] F. J. Muller, L. Isa, and J. Vermant. Toughening colloidal gels using rough building blocks. *Nat Commun*, 14(1):5309, 2023.

[2] Tuo Ji, Chi Ma, Logan Brisbin, Liwen Mu, Christopher G Robertson, Yalin Dong, and Jiahua Zhu. Organosilane grafted silica: Quantitative correlation of microscopic surface characters and macroscopic surface properties. *Applied Surface Science*, 399:565–572, 2017.

[3] Muhammad Zaman Khan, Vijay Baheti, Jiri Militky, Azam Ali, and Martina Vikova. Superhydrophobicity, uv protection and oil/water separation properties of fly ash/trimethoxy (octadecyl) silane coated cotton fabrics. *Carbohydrate polymers*, 202:571–580, 2018.

[4] Eoin Murray, Philip Born, Anika Weber, and Tobias Kraus. Synthesis of monodisperse silica nanoparticles dispersable in non-polar solvents. *Advanced Engineering Materials*, 12(5):374–378, 2010.

[5] Rickey D Badley, Warren T Ford, Frank J McEnroe, and Roger A Assink. Surface modification of colloidal silica. *Langmuir*, 6(4):792–801, 1990.

[6] Eliana Galland Barrera, Paolo R Livotto, and João HZ dos Santos. Hybrid silica bearing different organosilanes produced by the modified stöber method. *Powder Technology*, 301:486–492, 2016.

[7] Ziyang Chang and Yan Lu. Fabrication of superhydrophobic surfaces with cassie-baxter state. *Journal of Dispersion Science and Technology*, 43(8):1099–1111, 2022.

[8] Mingxin He, Johnathon P Gales, Xinhang Shen, Min Jae Kim, and David J Pine. Colloidal particles with triangular patches. *Langmuir*, 37(23):7246–7253, 2021.

[9] S. Ding, C. Zhang, W. Wei, X. Qu, J. Liu, and Z. Yang. Amphiphilic patchy composite colloids. *Macromol Rapid Commun*, 30(6):475–80, 2009.

[10] R Scott McLean and Bryan B Sauer. Tapping-mode afm studies using phase detection for resolution of nanophases in segmented polyurethanes and other block copolymers. *Macromolecules*, 30(26):8314–8317, 1997.

[11] Aaron PR Eberle, Norman J Wagner, Bulent Akgun, and Sushil K Satija. Temperature-dependent nanostructure of an end-tethered octadecane brush in tetradecane and nanoparticle phase behavior. *Langmuir*, 26(5):3003–3007, 2010.

[12] A. Kuijk, A. van Blaaderen, and A. Imhof. Synthesis of monodisperse, rodlike silica colloids with tunable aspect ratio. *J Am Chem Soc*, 133(8):2346–9, 2011.

[13] Michele Zanini, Chiao-Peng Hsu, Tommaso Magrini, Emanuele Marini, and Lucio Isa. Fabrication of rough colloids by heteroaggregation. *Colloids and Surfaces A: Physicochemical and Engineering Aspects*, 532:116–124, 2017.

[14] M. Das and G. Petekidis. Shear induced tuning and memory effects in colloidal gels of rods and spheres. *J Chem Phys*, 157(23):234902, 2022.

[15] Michael J. Solomon and Patrick T. Spicer. Microstructural regimes of colloidal rod suspensions, gels, and glasses. *Soft Matter*, 6(7), 2010.

[16] F. Bonacci, X. Chateau, E. M. Furst, J. Fusier, J. Goyon, and A. Lemaitre. Contact and macroscopic ageing in colloidal suspensions. *Nat Mater*, 19(7):775–780, 2020.

[17] Jacob B. Israelachvili. *Intermolecular and surface forces*. Elsevier, 2011.

[18] Hans-Jürgen Butt, Brunero Cappella, and Michael Kappl. Force measurements with the atomic force microscope: Technique, interpretation and applications. *Surface Science Reports*, 59(1-6):1–152, 2005.

[19] L. Yang and H. Therien-Aubin. Behavior of colloidal gels made of thermoresponsive anisotropic nanoparticles. *Sci Rep*, 12(1):12157, 2022.

[20] T. H. Besseling, M. Hermes, A. Kuijk, B. de Nijs, T. S. Deng, M. Dijkstra, A. Imhof, and A. van Blaaderen. Determination of the positions and orientations of concentrated rod-like colloids from 3d microscopy data. *J Phys Condens Matter*, 27(19):194109, 2015.

[21] Thomas Gibaud, Thibaut Divoux, and Sébastien Manneville. *Nonlinear Mechanics of Colloidal Gels: Creep, Fatigue, and Shear-Induced Yielding*, pages 1–24. Springer Berlin Heidelberg, Berlin, Heidelberg, 2020.

[22] U. Gasser and B. Zhou. Structural imperfections in amorphous metals. *Journal of Non-Crystalline Solids*, 31:207–211, 1978.

[23] Jan Mewis and Norman J. Wagner. *Colloidal Suspension Rheology*. Cambridge Series in Chemical Engineering. Cambridge University Press, 2011.

[24]

[25] Peter Schall, David A Weitz, and Frans Spaepen. Structural rearrangements that govern flow in colloidal glasses. *Science*, 318(5858):1895–1899, 2007.

[26] G. Pagani, M. Hofmann, L. E. Govaert, T. A. Tervoort, and J. Vermant. No yield stress required: Stress-activated flow in simple yield-stress fluids. *Journal of Rheology*, 68(2):155–170, 2024.

[27] T. A. Tervoort, E. T. J. Klompen, and L. E. Govaert. A multi-mode approach to finite, three-dimensional, nonlinear viscoelastic behavior of polymer glasses. *Journal of Rheology*, 40(5):779–797, 1996. doi: 10.1122/1.550755.

[28] E. T. J. Klompen and L. E. Govaert. Nonlinear viscoelastic behaviour of thermorheologically complex materials. *Mechanics of Time-Dependent Materials*, 3(1):49–69, 1999.

[29] R. A. Schapery. On the characterization of nonlinear viscoelastic materials. *Polymer Engineering Science*, 9(4):295–310, 1969.

[30] Aditya Jaishankar and Gareth H. McKinley. Power-law rheology in the bulk and at the interface: quasi-properties and fractional constitutive equations. *Proceedings of the Royal Society A: Mathematical, Physical and Engineering Sciences*, 469(2149):20120284, 2013.

[31] Jake Song, Niels Holten-Andersen, and Gareth H. McKinley. Non-maxwellian viscoelastic stress relaxations in soft matter. *Soft Matter*, 19(41):7885–7906, 2023.

[32] T. A. Tervoort, R. J. M. Smit, W. A. M. Brekelmans, and L. E. Govaert. A constitutive equation for the elasto-viscoplastic deformation of glassy polymers. *Mechanics of Time-Dependent Materials*, 1(3):269–291, 1997.

[33] Miroslav Grmela and Hans Christian Öttinger. Dynamics and thermodynamics of complex fluids. i. development of a general formalism. *Physical Review E*, 56(6):6620–6632, 1997. PRE.

[34] Markus Hütter and Theo A. Tervoort. Thermodynamic considerations on non-isothermal finite anisotropic elasto-viscoplasticity. *Journal of Non-Newtonian Fluid Mechanics*, 152(1):53–65, 2008.

[35] Christopher W. Macosko. *Rheology : principles, measurements, and applications.* Advances in interfacial engineering series. VCH, New York, NY, 1994.

[36] Jan Engmann, Colin Servais, and Adam S. Burbidge. Squeeze flow theory and applications to rheometry: A review. *Journal of Non-Newtonian Fluid Mechanics*, 132(1):1–27, 2005.

[37] Giovanni Volpe, Onofrio M Marago, and Halina Rubinsztein-Dunlop. Roadmap for optical tweezers 2023. *Journal of Physics: Photonics*, 2023.

[38] Eric M. Furst and John P. Pantina. Yielding in colloidal gels due to nonlinear microstructure bending mechanics. *Phys. Rev. E*, 75:050402, 5 2007.

[39] Francesco Bonacci, Xavier Chateau, Eric M Furst, Jennifer Fusier, Julie Goyon, and Anaël Lemaître. Contact and macroscopic ageing in colloidal suspensions. *Nature Materials*, 19(7):775–780, 2020.

[40] Ruixue Liang, Xia Fang, Biwei Qiu, and Hua Zou. One-step synthesis of golf ball-like thiol-functionalized silica particles. *Soft Matter*, 16:9113–9120, 10 2020.

[41] Philippa-Kate Andrew, Allan Raudsepp, Volker Nock, Daniel Fan, Martin A. K. Williams, Urs Staufer, and Ebubekir Avci. Developing an optical microlever for stable and unsupported force amplification. In *2022 International Conference on Manipulation, Automation and Robotics at Small Scales (MARSS)*, pages 1–8, 2022.

[42] Jader Colombo and Emanuela Del Gado. Stress localization, stiffening, and yielding in a model colloidal gel. *Journal of Rheology*, 58(5):1089–1116, 09 2014.

[43] Kathryn A Whitaker, Zsigmond Varga, Lilian C Hsiao, Michael J Solomon, James W Swan, and Eric M Furst. Colloidal gel elasticity arises from the packing of locally glassy clusters. *Nature communications*, 10(1):2237, 2019.

6 APPENDIX